CrossMark

AOPS: RECENT ADVANCES TO OVERCOME BARRIERS IN THE TREATMENT OF WATER, WASTEWATER AND AIR

Combination of sunlight, oxidants, and Ce-doped TiO₂ for phenol degradation

Marcela V. Martin[1] · Adriana Ipiña[1] · Paula I. Villabrille[2] · Janina A. Rosso[1]

Abstract The degradation of phenol was used as a model reaction to investigate the photocatalytic properties of cerium-doped (0.1 nominal atomic percent) TiO₂ catalysts in the presence and in the absence of oxidants: persulfate (PS) or hydrogen peroxide (HP). Experiments were performed in batch reactors using either artificial light (ultraviolet or visible) or solar exposure during spring–summer seasons in La Plata City (34.90° S, 57.92° W, 15 MASL). The formation of hydroquinone, catechol, and p-benzoquinone was observed in all the experiments. Additionally, for the experiments with PS (with or without *catalyst*), evidence of the formation of dimers and trimers was found. Total degradation of phenol (250 μM) was achieved with doped material and 7 mM of PS (*two doses*) after 3 h of solar exposure ($H^{S}_{UV, T} = 2.9 \pm 0.6\ 10^5$ J m^{-2}).

✉ Janina A. Rosso
janina@inifta.unlp.edu.ar

Marcela V. Martin
mmartin@inifta.unlp.edu.ar

Adriana Ipiña
iphadra@inifta.unlp.edu.ar

Paula I. Villabrille
paulav@conicet.gov.ar

[1] Instituto de Investigaciones Fisicoquímicas Teóricas y Aplicadas (INIFTA), CONICET, Universidad Nacional de La Plata (UNLP), 1900 La Plata, Argentina

[2] Centro de Investigación y Desarrollo en Ciencias Aplicadas (CINDECA), CONICET, Universidad Nacional de La Plata (UNLP), 1900 La Plata, Argentina

Introduction

Increased water pollution is a major concern worldwide. Among the contaminants found in surface water and groundwater, phenols and their derivatives are of environmental significance due to their toxicity.

Nowadays, research activities focus on the use of advanced oxidation processes (AOP) for the destruction of organic species resistant to conventional methods, such as phenolic compounds (Kudo et al. 2003). The application of heterogeneous photocatalytic water purification processes has gained wide attention due to its effectiveness in degrading and mineralizing recalcitrant organic compounds (Bahnemann 2004; Chong et al. 2010). By far, TiO₂ has played a much larger role in this scenario compared to other semiconductor photocatalysts because of its low cost, effectiveness, inert nature, and photostability.

The heterogeneous photocatalysis process begins with the generation of electron–hole pairs in the semiconductor particle. When a photon with energy $h\nu$ equal to or greater than the band gap energy of the semiconductor (E_{GAP}) shines on it, it promotes an electron (e$^-$) from the valence band (VB) to the conduction band (CB), generating a hole (h$^+$) in the valence band. These charge carriers, e$^-_{CB}$ and h$^+_{VB}$, can migrate to the semiconductor surface, getting caught on surface defects or reacting with an appropriate acceptor or electron donor. It is also possible that these charge carriers will recombine with each other, dissipating excess energy as heat (Hoffmann

🖄 Springer

et al. 1995). Furthermore, TiO_2 has the advantage of using solar ultraviolet radiation, because the energy gap between its valence and conduction bands (E_{GAP} close to 3 eV) allows photons with wavelength ~390 nm (near ultraviolet (UV)) to produce catalyst photon excitation. This provides important economic and ecological benefits by sustainable applications (Herrmann 1999; Malato et al. 2009).

However, the application of TiO_2 as catalysts for treating polluted water still presents a number of technical challenges. The increment of the photocatalytic activity in the visible region is the main focus of recent research. Several approaches for TiO_2 modification have been proposed: doping with metals, doping with nonmetals, co-doping technique, and surface organic modification.
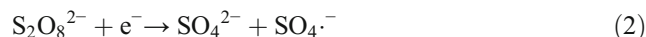
The effect of metal-ion dopants on the photocatalytic activity is a complex problem. The visible-light photoactivity of metal-doped TiO_2 can be explained by a new energy level produced in the band gap of TiO_2 by the dispersion of metal nanoparticles in the TiO_2 matrix. The electrons can be excited from the defect state to the TiO_2 conduction band by photons. An additional benefit of transition metal doping is the improved trapping of electrons to inhibit electron–hole recombination during irradiation. On the other hand, the synthesis of metal-doped TiO_2 is quite simple: TiO_2 particles can be substitutionally or interstitially doped with different cations and can form mixed oxides or a mixture of oxides. The dominant parameters include the method of doping (e.g., impregnation, coprecipitation, and sol–gel methods), the nature and concentration of dopants, and the thermal treatment applied (Dong et al. 2015).

Moreover, since surface sites can also be occupied by metal-ion dopants, the surface properties as well as the point of zero charge value of TiO_2 may be altered by doping, depending both on the type and amount of the dopant metal. Consequently, a modification of adsorption properties takes place. In particular, lanthanide ions can form complexes with various Lewis bases (e.g., acids, amines, aldehydes, alcohols, thiols, etc.) through interaction of these functional groups with the *f*-orbitals of lanthanides (Dong et al. 2015).
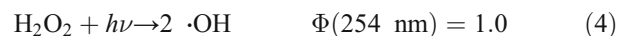
The modification of TiO_2 doped with Ce shows a significant potential to overcome the high charge carrier recombination that pristine TiO_2 particles present (Silva et al. 2009). Additionally, Ce incorporation into TiO_2 induces a red shift of the electronic absorption band, promoting the generation of e^-_{CB} and h^+_{VB} under visible-light irradiation (Sun et al. 2014; Martin et al. 2015).

Another strategy for an effective decontamination at relatively lower cost is the combination of UV/TiO_2 photooxidative degradation process with either physical or chemical operations (Augugliaro et al. 2006).

Inorganic additives provide electron scavengers such as hydrogen peroxide (H_2O_2, labeled as HP in this work) and persulfate ($S_2O_8^{2-}$, labeled as PS in this work) (Faisal et al. 2007) and trap electrons to generate more $\cdot$OH (Perkowski et al. 2003), reactions (1) to (3):

$$H_2O_2 + e^- \rightarrow \cdot OH + {}^-OH \quad (1)$$

$$S_2O_8{}^{2-} + e^- \rightarrow SO_4{}^{2-} + SO_4 \cdot^- \quad (2)$$

$$SO_4 \cdot^- + H_2O \rightarrow SO_4{}^{2-} + \cdot OH + H^+ \quad (3)$$

The presence of these electron acceptors enhanced the degradation rate by (i) preventing the electron–hole recombination by accepting the conduction band electron, (ii) increasing the hydroxyl radical concentration, and (iii) generating other oxidizing species ($SO_4^{\cdot-}$) to accelerate the intermediate compound oxidation rate (Madhavan et al. 2006). Additionally, HP and PS are able to undergo photocleavage of the *peroxo* bond yielding $SO_4^{\cdot-}$ or $\cdot$OH radicals, reactions (4) and (5), respectively (He et al. 2014; Luo et al. 2015; Sharma et al. 2016), contributing to the formation of free radicals (Φ indicates the quantum yield for each reaction).

$$H_2O_2 + h\nu \rightarrow 2 \cdot OH \qquad \Phi(254 \ nm) = 1.0 \quad (4)$$

$$S_2O_8{}^{2-} + h\nu \rightarrow 2SO_4 \cdot^- \qquad \Phi(254 \ nm) = 1.8 \quad (5)$$

However, HP and PS could act as scavengers of free radicals and reduce the global efficiency, depending on the experimental conditions.

In previous work, we reported that the addition of a low amount of cerium (0.1 nominal atomic percent) to TiO_2 catalysts increases the percentage of phenol degradation compared to that of undoped material (Martin et al. 2015). As far as we know, there are no previous studies on the effect of inorganic oxidants for that experimental condition, i.e., Ce-doped TiO_2 as catalyst.

The main aim of this work is the study of phenol degradation using Ce-doped TiO_2 catalysts in combination with oxidants (HP and PS) under artificial light (ultraviolet or visible) or solar exposure. Phenol was used as model of phenolic compounds, relevant pollutants of wastewater produced by chemical, petrochemical, food-processing, or biotechnological industries (Patel et al. 2014).

This investigation examines the disappearance rate of phenol, the formation of intermediates or by-products, and the degree of total mineralization of phenol. It also includes spectral solar irradiance measurements during the spring–summer period in the southern hemisphere (from October to February), simultaneously with the experiments, for comparison with artificial light sources.

Experimental section

Chemicals

The following specific commercial reagents were used in this study: phenol (Aldrich), sodium persulfate (Merck), and hydrogen peroxide (35 % v/v, Biopack).

A synthesized Ce-doped TiO_2 catalyst ($E_{GAP} = 2.80$ eV, $S_{BET} = 27.68$ m^2 g^{-1}) was used. The catalyst was prepared by the sol–gel method, modifying the procedure reported by Choi et al. (2010), with $Ce(NO_3)_3 6H_2O$ (Aldrich) as metal-ion precursor. The obtained xerogel was calcined at 600 °C in a programmable furnace to remove organic chemicals and to crystallize initial amorphous TiO_2 to anatase and rutile-phase TiO_2. The calcination was precisely controlled at a ramp rate of 6 °C min^{-1} and target temperature of 600 °C for 1 h, under air, followed by natural cooling down. The Ce-doped TiO_2 was prepared to give a doping level of 0.1 nominal atomic percent (at.%). The prepared material will be referred to hereafter as 0.1Ce (referring to 0.1 Ce nominal atomic percent). A more detailed description of the catalyst synthesis and its characterizations has been previously reported (Martin et al. 2015).

Photoreactors and experimental procedures

Artificial irradiation experiments

The oxidation of phenol in catalyst suspensions was carried out in a glass reactor (150 mL) at 25 °C, in air, and with continuous stirring. For each run, 100 mL of a reaction mixture of phenol 50 μM and catalyst 1 g L^{-1} was ultrasonically dispersed in the dark for 15 min. The effect of the addition of oxidants (HP and PS) to the reaction medium was evaluated. The amount of oxidant corresponding to the equimolar ratio required for the complete oxidation of phenol was defined as one dose. For these experiments, two doses were chosen (1.4 mM for 50 μM of phenol).

A Rayonet photoreactor RPR-100 (Southern New England Ultraviolet Company) with interchangeable lamps (ultraviolet or visible lamps with maximum emission at 365 or 575 nm, respectively) was used.

In the absence of oxidants, the evolution of phenol concentration with irradiation (without catalyst) and without irradiation (with catalyst) was monitored to check the direct photolysis and the adsorption of phenol on the material, respectively. Sampling was performed periodically.

Solar exposure experiments

The solar photocatalytic oxidation of phenol was carried out in 250-mL glass batch reactors of cylindrical geometry type (9 cm diameter), in air, and with continuous stirring to ensure that the material remained in suspension. For each run, the reaction mixture was prepared by ultrasonically dispersing 100 mg catalyst (1 g L^{-1}), 100 mL ultrapure water (Milli-Q: resistivity >18 MΩ cm and <20 ppb organic carbon), and the required amount of phenol to obtain concentrations of 50 and 250 μM, in the dark for 15 min. These experiments were performed in the absence and in the presence of HP and PS (one or two doses, as previously defined) using sunlight under outdoor conditions in La Plata City, Argentina. Sampling was performed as previously described.

Effect of temperature

To detect any influence of possible thermal effects, experiments with thermal activation of HP and PS were performed. The possibility of thermal decomposition of phenol was also checked.

The reaction mixtures were prepared in the same way as those for solar experiments. Then, they were incubated at 40 °C in the dark for 5 h. Sample aliquots were periodically collected to be analyzed.

Identification of by-products

Phenol concentration and intermediate products (catechol, hydroquinone, and p-benzoquinone) in the filtered samples were determined using HPLC (HP 1050 Ti series) with multiwavelength detection, a C18 Restek Pinnacle II column (particle size 5 μm, 2.1 mm, id 250 mm), and a 50/50, methanol/0.03 M H_3PO_4 mixture as eluent at 0.1 mL min^{-1} constant flux.

For a more effective monitoring of the degree of phenol mineralization (i.e., conversion to CO_2 and H_2O), total organic carbon (TOC) was determined. The total organic carbon was measured with a high-temperature carbon analyzer (Shimadzu TOC 5000 A) using a calibration curve with potassium biphthalate standard.

In order to identify solid by-products from the thermally activated PS experiment, they were dissolved in methanol and analyzed by LC–MS. Due to the small amount of solids formed in the experiment of phenol degradation with PS and 0.1Ce under UV irradiation, this assay was performed several times. The reaction mixtures were filtered, and the solids were washed with methanol. This methanolic extract was analyzed by LC–MS. The LC–MS equipment consists of a separative Agilent HPLC system, model 1100, with a C18 column and diode array detector (DAD) with a measuring range between 190 and 900 nm, coupled with a mass spectrometer, simple quadrupole, Agilent model VL. The mass spectrometer has a measurement range of masses from 100 to 1000 atomic mass units (amu), with a resolution of 1 amu and fragmenting variable energy

between 20 and 400 eV. We used an atmospheric pressure ionization (API) type, with ESI source at negative operation mode.

Samples of fresh and used catalysts (washed with water) were characterized by Fourier transform infrared spectroscopy (FTIR, Bruker IFS 66) to consider the possibility of reutilization of the catalyst.

Irradiance and radiant exposure determination

Spectral irradiance (E_λ) from artificial and natural sources was measured with a high-resolution Avantes spectrometer (AvaSpec-ULS3648 model). The device is connected to a fiber optic sensor, which includes a diffuser as cosine corrector and a computer linked through a USB2 interface cable. The equipment has a CCD detector linear array (3648 pixels) and slit-25. All the measurements were performed using the options Irradiance and Scope Mode, with reference and dark data. By adjusting the integration times and spectral average for optimal acquisition, it achieves a good signal according to source intensity (Ipiña et al. 2014).

Irradiance (E) is defined as the integration of E_λ with respect to wavelength on the interval [λ_1, λ_2]. However, transmittance and the spatial distribution light source must be considered to estimate the irradiance received by the solution ($E_{\Delta\lambda, T}$), after passing through the glass reactors. In this sense, the absorption spectra (A_λ) of glass reactors were recorded on a Shimadzu UV-1800 spectrophotometer. If the reflection or scattering is practically negligible, internal transmittance is represented as $T_\lambda = 10^{-A\lambda}$. The glass behaves as a notch filter, preventing the passage of radiation evenly. E_λ is multiplied by T_λ to obtain $E_{\lambda, T}$, i.e., spectral irradiance affected by transmittance. The last term represents an intensity value for each wavelength. Finally, irradiance reaching the solution is determined as

$$E_{\Delta\lambda, T} = \int_{\lambda_1}^{\lambda_2} E_{\lambda, T}\, d\lambda \tag{6}$$

The result is expressed in units of watts per square meter for a whole range of wavelengths, where $\Delta\lambda$ could be 290–400 nm (ultraviolet, UV) or 400–750 nm (visible, VIS). This procedure was applied to all measurements, hereafter denoted as $E^S_{UV, T}$ and $E^S_{VIS, T}$ from sunlight and $E^L_{UV, T}$ and $E^L_{VIS, T}$ derived from an artificial source. On the other hand, radiant exposure (H) is defined as $E_{\Delta\lambda, T}$ integrated over the irradiation time, and the SI unit is joules per square meter (Braslavsky 2007). Afterwards, $H^S_{UV, T}$, $H^S_{VIS, T}$, $H^L_{UV, T}$, and $H^L_{VIS, T}$ were derived according to the convention adopted.

Artificial irradiance

The artificial irradiation system has a cylindrical arrangement of the lamps where reactions and E_λ measurements were performed. The spectrometer sensor was mounted and surrounded by four pairs of lights (of the same type), equally spaced. One way to assess the spatial variation of spectral irradiance on a path of 2π was with fiber optics directly focused on the lamps attached to a cylinder wall. All measurements were recorded tracing a trajectory around the glass container. In this case, the glass reactor prevents the passage of radiation below 275 nm. The UV and VIS lamps have local maximum intensity at 365 and 575 nm, respectively (as shown in Fig. 1).

Using the above-described method to calculate the received irradiance, the results were interpolated as a function of angle. Figure 2 shows $E^L_{UV, T}$ behavior in polar coordinates, inside the reactor. It can be observed that the intensity varies with position, as expected. At fixed height and radius ($h = 13$ cm and $r = 7$ cm), maximum irradiances are located in front of each pair of lamps (at positions 0°, 90°, 180°, 270°). The value of $E^L_{VIS, T}$ was also deduced, and a similar performance was found. Although irradiance depends on distance, a reasonable approximation can be supported statistically taking into account the values acquired on the outline of the cross-sectional area. Then, the mean values were $E^L_{UV, T} = 28 \pm 3$ W m^{-2} and $E^L_{VIS, T} = 20 \pm 1$ W m^{-2}. Assuming that the intensity did not change for 5 h in this system, the quantities of irradiances received are multiplied by the irradiation time. The radiant exposure values were $H^L_{UV, T} = 1.0 \pm 0.1 \ 10^5$ J m^{-2} and $H^L_{VIS, T} = 7.2 \pm 0.3 \ 10^4$ J m^{-2} per hour.
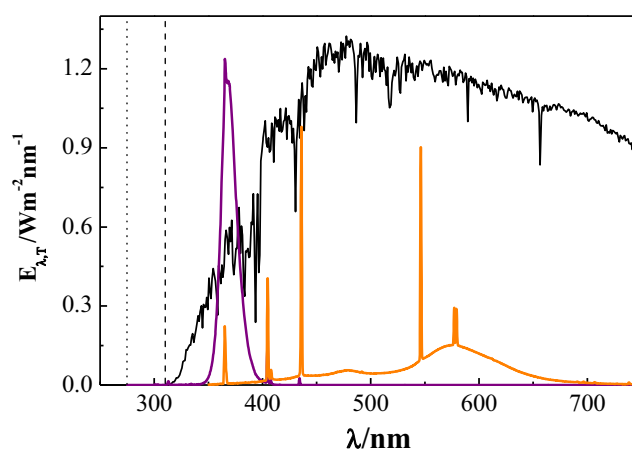

Fig. 1 Spectral irradiance measurements affected by glass transmittances ($E_{\lambda, T}$): at solar noon in La Plata City on October 8, 2014 (*black curve*) and facing UV and VIS lamps (*purple and orange curves*) at the reactor center. The *dotted and dashed lines* at 275 and 310 nm represent the transmittance cutoffs of the glass container for artificial light and solar exposure experiments, respectively
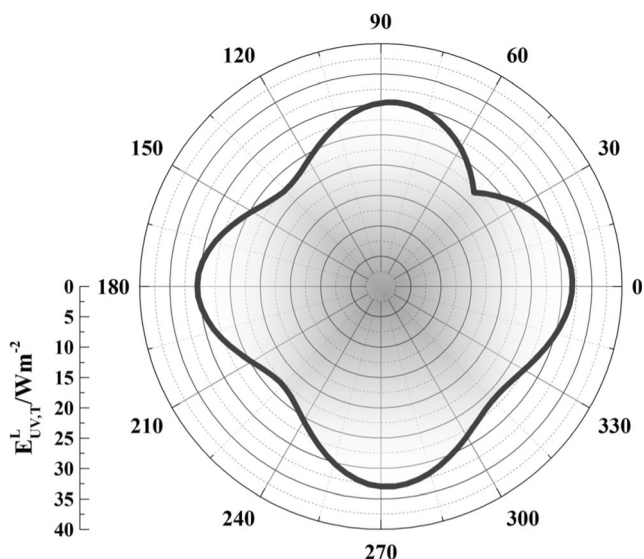
Fig. 2 $E^{L}_{UV,\,T}$ derived from measurements on circular contour at fixed height and radius ($h = 13$ cm and $r = 7$ cm), inside the reactor. The lamps were distributed in pairs at locations: 0°, 90°, 180°, and 270°

Solar irradiance

The experiments in the outdoor condition were conducted in the spring and summer periods of the southern hemisphere. The reaction mixtures were exposed to sunlight on a horizontal platform located in La Plata City, Argentina (34.90° S, 57.92° W, 15 MASL). The local time (LT) is given by universal time minus 3 h, and solar noon ranged from 12:39 p.m. to 01:05 p.m. in the geographical position and seasons established. The reaction mixtures were exposed in clear-sky days, for a period of 5 h, centered around solar noon. This exposure time was chosen for the purpose of comparing the energy received per unit surface ($H^{S}_{UV,\,T}$ and $H^{S}_{VIS,\,T}$) in the same irradiation time used in an artificial device.

The transmittance (T_{λ}) of the glass cover that protects the solutions was quantified previously, allowing the passage of radiation at $\lambda > 310$ nm. Simultaneously with the exposure routine, the Avantes spectrometer recorded the E_{λ} data. Measurements were carried out throughout the day (from 10 a.m. to 4 p.m. LT). The tropospheric ultraviolet and visible (TUV) model (Madronich 1995) was applied as control. Several solar spectrum measurements at the place had been previously compared with TUV model values and showed a good agreement between them (Ipiña et al. 2014). As an example, the solar spectrum (corresponding to October 8, 2014) is displayed in Fig. 1. Subsequently, by means of Eq. (6), $E^{S}_{VIS,\,T}$ and $E^{S}_{UV,\,T}$ were determined during the day. In general, under a cloudless sky or with wispy clouds, the solar irradiance (either UV or VIS range) has a Gaussian behavior, and the daily maximum value is reached at solar noon. The maximum irradiance data are taken into account as reference and are reported for each day of measurement. In this case,

source intensity varies along the hours of the day. Finally, using the method mentioned above and solving the integral of $E^{S}_{VIS,\,T}$ and $E^{S}_{UV,\,T}$ as a function of exposure time, $H^{S}_{VIS,\,T}$ and $H^{S}_{UV,\,T}$ were computed every hour.

Results and discussion

Degradation of phenol with artificial light sources

In the presence of 0.1Ce, without irradiation (in the dark), no significant differences between experimental and analytical concentrations were observed after 3 h, indicating that the adsorption of phenol on this material was negligible.

The effects of irradiation with two different light sources (UV or VIS lamps) on phenol degradation in the absence and in the presence of 0.1Ce catalyst and/or the addition of oxidants were investigated. The corresponding results are shown in Fig. 3 (UV lamps, total radiant exposure 3.0 ± 0.3 10^{5} J m^{-2}) and Fig. 4 (VIS lamps, total radiant exposure 3.6 ± 0.2 10^{5} J m^{-2}). Table 1 shows the final percentages of degradation of phenol for the studied systems.
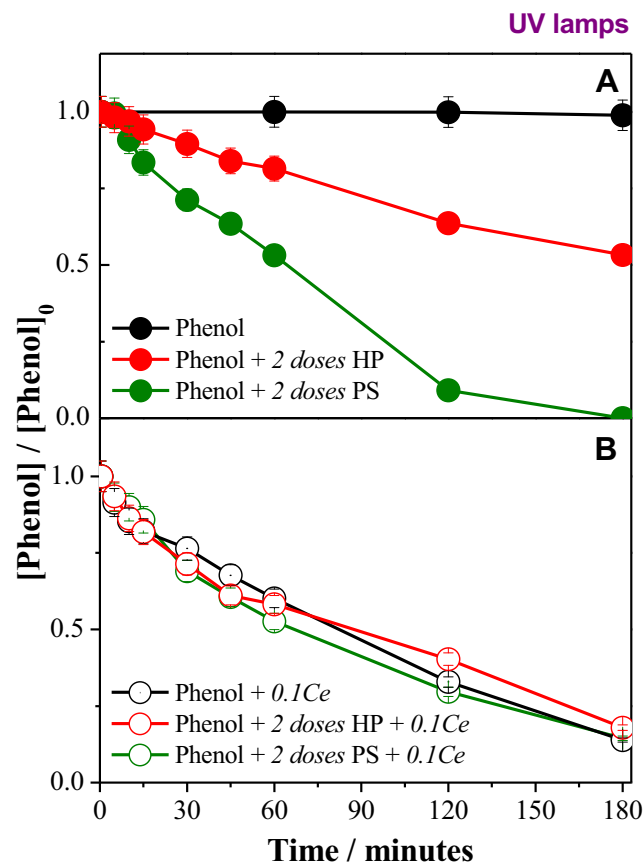

Fig. 3 Degradation of phenol 50 μM after 3 h with UV lamps (total radiant exposure 3.0 ± 0.3 10^{5} J m^{-2}), in the presence and in the absence of oxidants, *A* without 0.1Ce catalyst and *B* with 0.1Ce catalyst (1.0 g L^{-1})
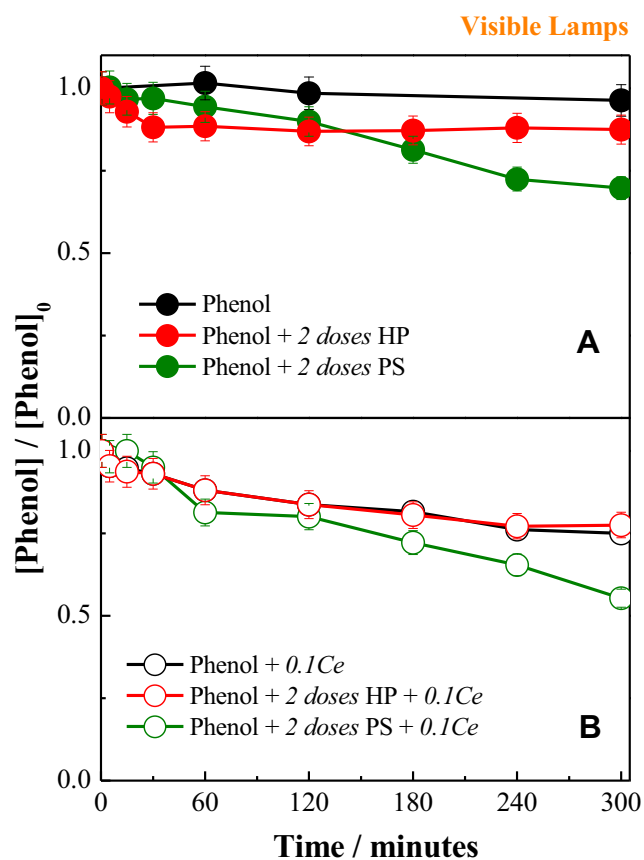
Fig. 4 Degradation of phenol 50 μM after 5 h with VIS lamps (total radiant exposure $3.6 \pm 0.2 \cdot 10^5$ J m^{-2}), in the presence and in the absence of oxidants, *A* without 0.1Ce catalyst and *B* with 0.1Ce catalyst (1.0 g L^{-1})

The photodegradation of phenol (without 0.1Ce catalyst or oxidants) was negligible after irradiation for 3 h with the UV lamps (Fig. 3(A)) or 5 h with the VIS lamps (Fig. 4(A)).

Under UV irradiation, PS treatment shows better results than HP treatment, reaching total degradation after 3 h. This difference was less important for VIS lamp irradiation, due to the small contribution of these lamps in the UV range (see spectrum in Fig. 1). As previously mentioned, both oxidants are able to yield free radicals (SO$_4^{\cdot-}$ or $\cdot$OH). However, the radical formation quantum yield of PS by UV (254 nm) in

Table 1 Percentages of phenol degradation ([phenol]$_0$ = 50 μM) by artificial irradiation for the studied systems

Treatment	% Degradation	
	UV lamps (3 h)	VIS lamps (5 h)
Phenol + 0.1Ce	87 ± 2	25 ± 2
Phenol + 2 doses HP	47 ± 2	12 ± 2
Phenol + 2 doses HP + 0.1Ce	83 ± 2	23 ± 2
Phenol + 2 doses PS	100 ± 2	30 ± 2
Phenol + 2 doses PS + 0.1Ce	86 ± 2	44 ± 2

oxygen-saturated water (1.8) is much higher than that of HP (1.0) (He et al. 2014). Then, the observed degradation of phenol was in line with the radical quantum yields of PS and HP.

In the presence of 0.1Ce and irradiation (without oxidant), phenol was almost completely degraded after irradiation for 3 h with the UV lamps, while just 25 % of degradation was obtained after 5 h with the VIS lamps (see Figs. 3(B) and 4(B)).

The combination of 0.1Ce with PS or HP allows an alternative path of reaction for the e$^-_{CB}$ generated in the catalyst, which reacts with the PS and HP yielding SO$_4^{\cdot-}$ or $\cdot$OH radicals, respectively. Free radicals could react with phenol enhancing its degradation, but could also be lost by undesirable reactions (reaction with the oxidant at higher concentration or recombination).

Treatments with 0.1Ce catalyst (alone or with the addition of oxidants) did not present significant differences in phenol degradation under UV lamp irradiation (Fig. 3b), while when using the VIS lamps, the combination of 0.1Ce catalyst and PS caused a slight improvement over 0.1Ce or 0.1Ce with HP (Fig. 4(B)).

These observations indicate that the use of two doses of PS with UV lamp irradiation was the faster method for phenol degradation. However, to evaluate the treatment performance, product formation has to be considered.

Possible by-products were analyzed. The formation of hydroquinone, catechol, and *p*-benzoquinone was observed in all the cases.

Additionally, for the experiments with PS (with or without 0.1Ce), an HPLC peak with longer retention time was detected, and the formation of a brownish solid was also observed. Similar behavior was reported for the degradation of phenol with thermally activated PS. Mora et al. (2011) assigned this to the formation of dimers (or phenylphenol or biphenyls).

In order to identify these products, the solids obtained from the experiments of phenol degradation with PS and 0.1Ce under UV irradiation and from thermally activated PS were analyzed by LC–MS. Both samples presented the same MS spectrum with three peaks. The peaks with $m/z = 277$ and 185 were assigned to the trimer and dimer of phenol, respectively. The peak with $m/z = 291$ could not be assigned to compounds related to phenol. The distinction between isomeric compounds could not be made with our equipment.

A remarkable fact is that treatments with similar rate of phenol degradation (see Fig. 3b) generated different products, and their consequences have to be considered to evaluate the applicability of the treatment.

The formation of solid compounds should be carefully analyzed for their possible effect on the reutilization of the catalyst. Under our experimental conditions, the obtained solid was partially soluble in water. Moreover, the FTIR spectra of fresh and used catalysts (washed six times with water and

dried out at 50 °C) were similar, indicating that a neglected amount of organic compounds could remain adsorbed on the catalyst after water washing, as shown in ESM 1 (Electronic Supplementary Material 1).

The efficiency observed with artificial light irradiation indicates promising results with solar exposure.

Solar experiments

In order to compare the results obtained from artificial sources, an initial phenol concentration of 50 µM was included in the outdoor experiments. Total degradation of phenol was achieved after 3 h under sunlight ($H^S_{VIS,\ T} = 4.2 \pm 0.9$ 10^6 J m^{-2}, $H^S_{UV,\ T} = 3.5 \pm 0.8$ 10^5 J m^{-2}).

We considered it necessary to determine the contribution of each spectral region. In this way, the radiant exposure values were calculated separately for each spectral range (UV or visible), and the degradation rate was plotted as a function of the radiant exposure values. The results corresponding to the artificial sources and sunlight experiments are shown in Fig. 5(A and B), due to the UV and VIS ranges, respectively.

The behavior of the degradation rate between the irradiation lamps and solar exposure suggests that the UV part of the spectrum was the most relevant for the photocatalytic process. However, the efficiency with solar exposure was slightly higher than that with the UV lamps, possibly due to VIS and thermal contributions, reaching total degradation at a shorter time than with the UV lamps. Taking into account these results, the initial concentration of phenol was increased up to 250 µM and the exposure time to 5 h.

Phenol concentration in aqueous solution (without catalyst) under solar radiation was monitored as control experiment ([phenol]$_0$ = 250 µM). After 5 h of continuous exposure to the sun (values of energy accumulated per unit surface during

Table 2 Percentages of phenol degradation and mineralization ([phenol]$_0$ = 250 µM) in the presence of 0.1Ce 1.0 g L^{-1}, with the addition of two different oxidants (HP and PS) at different doses, after 5 h of reaction ($H^S_{UV,\ T} = 4.8 \pm 0.6$ 10^5 J m^{-2})

Treatment	% Degradation[a]	% Mineralization[b]
Phenol + 0.1Ce	75 ± 2	44 ± 2
Phenol + 2 doses HP	43 ± 2	36 ± 2
Phenol + 2 doses HP + 0.1Ce	82 ± 2	78 ± 2
Phenol + 1 dose HP + 0.1Ce	71 ± 2	67 ± 2
Phenol + 2 doses PS	100 ± 2	98 ± 2
Phenol + 2 doses PS + 0.1Ce	100 ± 2	99 ± 2
Phenol + 1 dose PS + 0.1Ce	83 ± 2	62 ± 2

[a] Percentages calculated from phenol concentration values determined by HPLC
[b] Percentages calculated from the measured values of total organic carbon (TOC)

this interval time: $H^S_{VIS,\ T} = 5.9 \pm 0.3$ 10^6 J m^{-2}, $H^S_{UV,\ T} = 4.8 \pm 0.6$ 10^5 J m^{-2}), no degradation was observed.

During solar experiments, the temperature measured reached a maximum value of 40 °C. Then, to detect any influence of possible thermal effects induced by solar light, experiments of thermal activation (in the dark) of 0.1Ce, HP, and PS were performed. The evolution of phenol concentration ([phenol]$_0$ = 250 µM) in aqueous solution at 40 °C in the presence of 0.1Ce alone or HP (with and without 0.1Ce) showed negligible degradation (around 3 %). However, the addition of PS (with or without catalyst) increased the degradation of phenol (15 %), indicating that this process has to be considered in solar exposure experiments.

The percentages of degradation and mineralization at the end of each treatment under solar exposure are listed in Table 2.
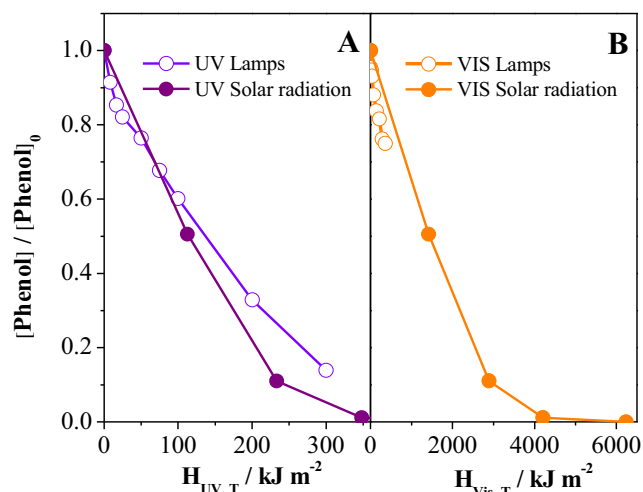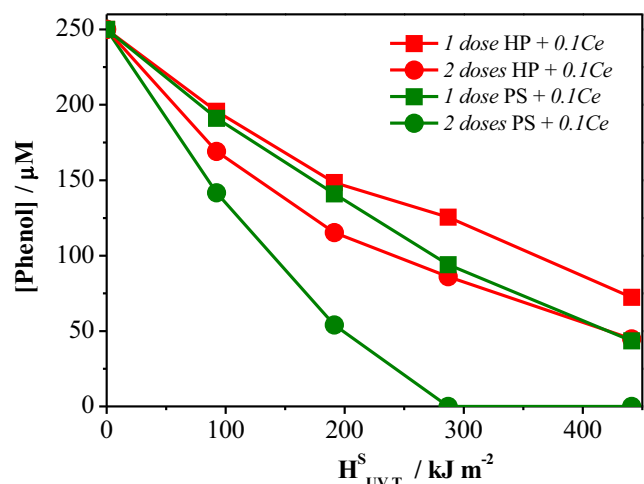

Fig. 5 Degradation of phenol 50 µM with 0.1Ce catalyst (1.0 g L^{-1}) as a function of the radiant exposure values: comparison between UV lamps and $H^S_{UV,\ T}$ after 3 h (*A*) and between VIS lamps and $H^S_{VIS,\ T}$ after 5 h (*B*)

Fig. 6 Disappearance of phenol as a function of solar exposure in the presence of 0.1Ce and HP or PS. Reaction conditions: catalyst 0.1Ce = 1.0 g L^{-1}, [phenol]$_0$ = 250 µM, PS or HP = 1 or 2 doses

The use of 0.1Ce alone showed a good degradation of phenol (75 % after 5 h of solar exposure treatment), while the mineralization reached 44 %. The behavior of HP or PS (two doses, 5 h solar exposure) was the same as with UV lamps: the efficiency of phenol degradation followed the order HP < 0.1Ce < PS.

Phenol degradation and mineralization improved when HP or PS was added to 0.1Ce (see Table 2). As shown in Fig. 6, the best results were obtained using two doses of oxidant. Total phenol degradation was achieved after 3 h of solar exposure ($H^S_{UV, T} = 2.9 \pm 0.6 \ 10^5$ J m^{-2}) using 0.1Ce and two doses of PS.

The solar experiments showed the formation of hydroquinone, catechol, and p-benzoquinone as reaction intermediates. Additionally, from treatments with PS (with or without 0.1Ce), an HPLC peak with longer retention time was detected, and the formation of a small quantity of brownish solids was observed, as in the experiments performed using PS and artificial light. Although no identification of these compounds was performed, we assume that they could be similar to the characterized products from PS and UV lamp experiments.

Conclusion

The use of the catalyst doped with Ce (0.1 at.%) is suitable for the degradation of phenol in aqueous phase, with sunlight (October to February, southern hemisphere).

The addition of oxidants (HP or PS) to the catalyst increases the process efficiency, achieving both degradation and mineralization of the contaminant.

The optimum result was obtained working with the catalyst and two doses of PS: total degradation of 250 µM phenol after 3 h of solar exposure ($H^S_{UV, T} = 2.9 \pm 0.6 \ 10^5$ J m^{-2}).

To evaluate the applicability of these methods, the nature of intermediates and by-products has to be considered.

The formation of hydroquinone, catechol, and p-benzoquinone was observed in all the experiments. These compounds are easily oxidized by $SO_4^{\cdot -}$ and $\cdot OH$ radicals, and total mineralization is possible by increasing the exposure time.

On the other hand, evidence of dimer and trimer formation was found in the experiments with PS (with or without 0.1Ce). The presence of solid by-products is a technical problem: solids (catalyst and products) have to be separated by filtration or centrifugation of the reaction mixture. However, the catalyst could be recovered by several water washes because these products are slightly soluble in water.

Finally, it is advised that the toxicity of intermediates and by-products should be investigated to evaluate the applicability of these methods. Future work is planned in order to explore these limitations.

References

Augugliaro V, Litter M, Palmisano L, Soria J (2006) The combination of heterogeneous photocatalysis with chemical and physical operations: a tool for improving the photoprocess performance. J Photochem Photobiol C 7:127–144

Bahnemann D (2004) Photocatalytic water treatment: solar energy applications. Sol Energy 77(5):445–459

Braslavsky SE (2007) Glossary of terms used in photochemistry, 3rd edition (IUPAC recommendations 2006). Pure Appl Chem 79:293–465

Choi J, Park H, Hoffmann MR (2010) Effects of single metal-ion doping on the visible-light photoreactivity of TiO$_2$. J Phys Chem C 114:783–792

Chong MN, Jin B, Chow CWK, Saint C (2010) Recent developments in photocatalytic water treatment technology: a review. Water Res 44:2997–3027

Dong H, Zeng G, Tang L, Fan C, Zhang C, He X, He Y (2015) An overview on limitations of TiO$_2$ based particles for photocatalytic degradation of organic pollutants and the corresponding countermeasures. Water Res 79:128–146

Faisal M, Tariq MA, Muneer M (2007) Photocatalysed degradation of two selected dyes in UV-irradiated aqueous suspensions of titania. Dyes Pigments 72:233–239

He X, de la Cruz AA, O'Shea KE, Dionysiou DD (2014) Kinetics and mechanisms of cylindrospermopsin destruction by sulfate radical-based advanced oxidation processes. Water Res 63:168–178

Herrmann JM (1999) Heterogeneous photocatalysis: fundamentals and applications to the removal of various types of aqueous pollutants. Catal Today 53:115–129

Hoffmann MR, Martin ST, Choi W, Bahnemann DW (1995) Environmental applications of semiconductor photocatalysis. Chem Rev 95:69–96

Ipiña A, Castaño C, Dántola ML, Thomas AH (2014) Solar radiation exposure of dihydrobiopterin and biopterin in aqueous solution. Sol Energy 109:45–53

Kudo T, Nakamura Y, Ruike A (2003) Development of rectangular column structured titanium oxide photocatalysts anchored on silica sheets by a wet process. Res Chem Intermed 29:631–639

Luo C, Ma J, Jiang J, Liu Y, Song Y, Yang Y, Guan Y, Wu D (2015) Simulation and comparative study on the oxidation kinetics of atrazine by UV/H$_2$O$_2$. UV/HSO$_5^-$ and UV/S$_2$O$_8^{2-}$. Water Res 80:99–108

Madhavan J, Muthuraaman B, Murugesan S, Anandan S, Maruthamuthu P (2006) Peroxomonosulphate, an efficient oxidant for the photocatalysed degradation of a textile dye, acid red 88. Sol Energ Mat Sol C 90:1875–1887

Madronich S (1995) The radiation equation. Nature 377(6551):682–683

Malato S, Fernández-Ibáñez P, Maldonado MI, Blanco J, Gernjak W (2009) Decontamination and disinfection of water by solar photocatalysis: recent overview and trends. Catal Today 147:1–59

Martin MV, Villabrille PI, Rosso JA (2015) The influence of Ce doping of titania on the photodegradation of phenol. Environ Sci Pollut Res 22:14291–14298

Mora VC, Rosso JA, Mártire DO, Gonzalez MC (2011) Phenol depletion by thermally activated peroxydisulfate at 70°C. Chemosphere 84(9): 1270–1275

Patel N, Jaiswal R, Warang T, Scarduelli G, Dashora A, Ahuja BL, Kothari DC, Miotello A (2014) Efficient photocatalytic degradation of organic water pollutants using V–N-codoped TiO_2 thin films. Appl Catal B Environ 150–151:74–81

Perkowski J, Bzdon S, Bulska A, Jóźwiak WK (2003) Decomposition of detergents present in car-wash sewage by titania photo-assisted oxidation. Polish J Environ Stud 15:457–465

Sharma J, Mishra IM, Kumar V (2016) Mechanistic stud y of photo-oxidation of bisphenol-A (BPA) with hydrogen peroxide (H_2O_2) and sodium persulfate (SPS). J Environ Manag 166:12–22

Silva AMT, Silva CG, Dražić G, Faria JL (2009) Ce-doped TiO_2 for photocatalytic degradation of chlorophenol. Catal Today 144:13–18

Sun P, Liu L, Cui S-C, Liu J-G (2014) Synthesis, characterization of Ce-doped TiO_2 nanotubes with high visible light photocatalytic activity. Catal Lett 144:2107–2113